Temporal compression mediated by short-term synaptic plasticity

Christian Leibold*[†‡§], Anja Gundlfinger[†‡], Robert Schmidt*[‡], Kay Thurley*[¶], Dietmar Schmitz[†‡], and Richard Kempter*[†‡]

*Institute for Theoretical Biology, Department of Biology, Humboldt-Universität zu Berlin, Invalidenstrasse 43, 10115 Berlin, Germany; [†]Neuroscience Research Center, Charité - Universitätsmedizin Berlin, Charitéplatz 1, 10117 Berlin, Germany; and [‡]Bernstein Center for Computational Neuroscience Berlin, Philippstrasse 13, 10115 Berlin, Germany

Edited by Nancy J. Kopell, Boston University, Boston, MA, and approved January 19, 2008 (received for review September 13, 2007)

Time scales of cortical neuronal dynamics range from few milliseconds to hundreds of milliseconds. In contrast, behavior occurs on the time scale of seconds or longer. How can behavioral time then be neuronally represented in cortical networks? Here, using electrophysiology and modeling, we offer a hypothesis on how to bridge the gap between behavioral and cellular time scales. The core idea is to use a long time constant of decay of synaptic facilitation to translate slow behaviorally induced temporal correlations into a distribution of synaptic response amplitudes. These amplitudes can then be transferred to a sequence of action potentials in a population of neurons. These sequences provide temporal correlations on a millisecond time scale that are able to induce persistent synaptic changes. As a proof of concept, we provide simulations of a neuron that learns to discriminate temporal patterns on a time scale of seconds by synaptic learning rules with a millisecond memory buffer. We find that the conversion from synaptic amplitudes to millisecond correlations can be strongly facilitated by subthreshold oscillations both in terms of information transmission and success of learning.

hippocampus | temporal coding | oscillations | tempotron

Time scales of cortical neuronal dynamics are mostly in the range of few milliseconds to hundreds of milliseconds and are imposed on through cellular properties (1, 2), the kinetics of synaptic transmission (3), and complex connectivity patterns (4). These time scales are well adjusted to the time window for the induction of synaptic changes via spike-timing-dependent synaptic plasticity (5–7), which leads to the hypothesis that synaptic plasticity provides a means of learning to discriminate and recognize distinct cellular activity patterns. In contrast to cellular phenomena, the time scales of behavioral and cognitive phenomena, such as navigation in a maze or short-term memory, are in the order of seconds or longer. How to transfer the resulting slow behaviorally evoked temporal patterns to synaptic long-term changes and enable the formation of long-term memories is, however, largely unclear.

The present article proposes a new mechanism that uses short-term synaptic plasticity to encode temporal stimulus properties via variable amplitudes of synaptic currents. The memory time scales of short-term synaptic plasticity are in the range from hundreds of milliseconds to several seconds (8, 9) and thus provide a potential memory buffer on a behavioral time scale. It is described how the distribution of synaptic amplitudes resulting from short-term plasticity can be efficiently transferred into a temporal spike code that represents the slow input patterns. This mechanism thus constitutes a temporal compression from seconds to milliseconds. Using experimental and modeling investigations, we demonstrate how the combination of short-term synaptic plasticity and subthreshold membrane potential oscillations serves to generate an information-efficient temporal spike code (*cf.* ref. 10). For hippocampal CA3 pyramidal cells *in vitro*, we measure the temporal range of delays between excitatory postsynaptic currents (EPSCs) and action potentials (APs) varying the amplitude of a simulated synaptic input. Next, using a computational model, we reproduce the results of the *in vitro* approach and calculate how much information about the input amplitude is conveyed via AP timing. Finally, we verify that the proposed mechanism is suitable for learning and decoding in downstream structures.

Results

Range of Delays Between Simulated EPSCs and APs. Synaptically induced currents determine the timing of a neuronal APs. In general, a large excitatory input current elicits a faster increase of the neuronal membrane potential than a small one. Thus, strong inputs give rise to shorter spike latencies than weak inputs and, consequently, the amplitudes of EPSCs are encoded in the timing of the APs. In this context, we first determined the temporal coding capabilities of APs triggered by varying EPSC input: For that, we measured the AP responses of a CA3 pyramidal cell induced by simulated EPSC sequences with increasing amplitudes (Fig. 1). These EPSC sequences are to represent the prominent short-term facilitation of single mossy fiber synapses evoking EPSCs with amplitudes from few tens of picoamperes to hundreds of picoamperes (for EPSC kinetics and amplitudes, see *Materials and Methods* and refs. 11–13). In addition to the simulated EPSCs, we imposed subthreshold oscillations with a frequency of 9 Hz, which is in the hippocampal theta band (4–12 Hz). Hippocampal theta oscillations are apparent in the extracellular field potential of freely behaving animals (14) and are also reflected through oscillations of the cellular membrane potential in anesthetized (15, 16) and behaving animals (17). Several repetitions of the stimulus train evoked a reliable pattern of postsynaptic APs (Fig. 1*A1*). The time delay between the onset of the EPSC and the postsynaptic AP ranged from 10.7 ± 0.3 ms (mean ± SEM) for high EPSC amplitudes to 63 ± 2 ms for low EPSC amplitudes (Fig. 1*B*). For $n = 10$ cells, the average time delay between the onset of the EPSC and the postsynaptic AP ranged from 11 ± 2 ms to 63 ± 2 ms, providing a temporal coding range of 51 ± 2 ms (Fig. 1*C1*), which is approximately half of a theta period. The temporal coding range with subthreshold oscillations is significantly enhanced (t test: $P < 10^{-4}$) compared with experiments without oscillations [Fig. 1 in supporting information (SI) *Appendix*].

NEUROSCIENCE

Determinants of Temporal Coding. Given subthreshold membrane potential oscillations, the temporal range of AP delays is a result of the interplay between oscillatory input and EPSC. In particular, the

Author contributions: C.L., A.G., D.S., and R.K. contributed equally to this work; C.L., A.G., D.S., and R.K. designed research; C.L., A.G., R.S., K.T., D.S., and R.K. performed research; C.L. and A.G. analyzed data; and C.L., A.G., R.S., D.S., and R.K. wrote the paper.

The authors declare no conflict of interest.

This article is a PNAS Direct Submission.

[§]To whom correspondence should be addressed at the present address: Department of Biology II, University of Munich, Grosshaderner Strasse 2, 82152 Planegg-Martinsried, Germany. E-mail: leibold@bio.lmu.de.

[¶]Present address: Institute of Physiology, University of Bern, Bühlplatz 5, 3012 Bern, Switzerland.

This article contains supporting information online at www.pnas.org/cgi/content/full/0708711105/DC1.

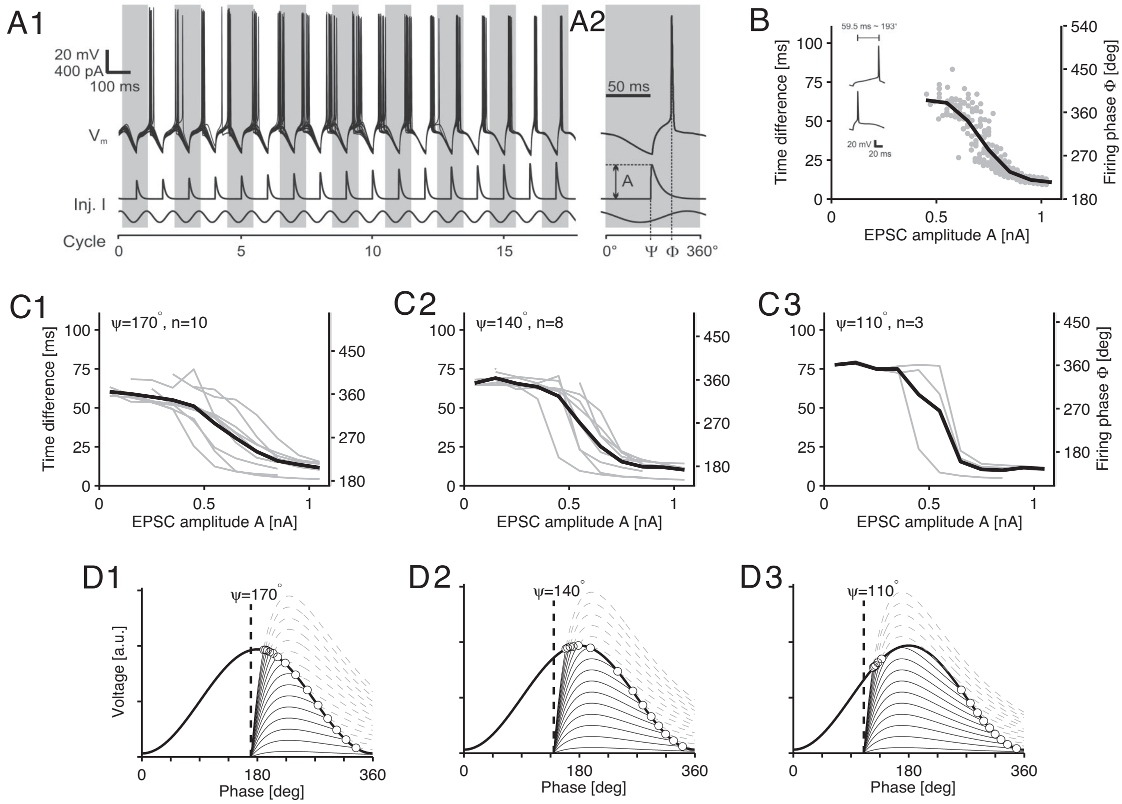

Fig. 1. Temporal coding range due to variations in EPSC amplitude and subthreshold oscillations. (*A1*) Voltage traces of a hippocampal CA3 pyramidal cell show an overlay of 16 repetitions of a current stimulus (Inj. I) that combines simulated EPSCs of increasing amplitude and an oscillatory current. The amplitude *A* of the injected EPSC was set to 300 pA in the first cycle and increased by 20 pA per cycle. The EPSC phase was set to 170° with respect to the subthreshold voltage oscillations. In this example, the phase of the current oscillation is shifted against that of the voltage oscillation by 50°. (*A2*) Magnification of cycle 15. At the input phase ψ, the simulated EPSC with amplitude *A* is applied. At the AP phase Φ, an AP is elicited. (*B*) Temporal delays (gray dots) between EPSC onset and AP in the same cell as in *A*. The black line depicts the mean delay between EPSCs and APs averaged over amplitude intervals of 0.1 nA. The resulting mean range of delays (temporal coding range) amounts to approximately half a cycle. (*Inset*) Single APs evoked by small (cycle 2) and large (cycle 16) EPSCs. (*C*) Mean delays (gray lines) averaged over several cells for three different input phases (170°, 140°, and 110°) that are corrected for pooling across cells by a phase shift of 60° (see *Materials and Methods*). Black lines depict the population mean. (*D*) In a schematic model, the temporal AP pattern can be illustrated by the points of intersection (white circles) between an oscillatory threshold (thick lines) and EPSPs with varying amplitudes. For input phase (dashed line) $\psi = 170°$ (*D1*), we expect a smooth dependence of firing phase on EPSC amplitude, whereas, for $\psi = 110°$ (*D3*), we expect a gap in the firing phases.

mechanism is sensitive to the oscillation frequency and amplitude, the input phase ψ, and the range of amplitudes *A* of the imposed EPSCs (Fig. 1*A2*). In what follows, the oscillation amplitude and frequency are kept constant at values typically observed during hippocampal theta oscillations (*Materials and Methods* and refs. 15–17). Changes in stimulus frequency do not alter the general outcome (SI Fig. 2 in *SI Appendix*). The influence of the input phase ψ on the firing phase Φ as a function of the EPSC amplitude *A* is illustrated in Fig. 1 *C* and *D* for three different input phases. An input phase $\psi = 170°$ results in only little curvature of the so-called "transfer function" $\Phi\psi(A)$. The resulting range of delays covers an interval of $\approx$50 ms. For an earlier input phase of $\psi = 110°$, the transfer function is strongly curved, yet the obtained delay range amounts to $\approx$70 ms. Temporal encoding of EPSC amplitudes is thus either almost-linear with a low coding range, or strongly curved with a large coding range (*cf.* Fig. 2*A* and ref. 18).

Although the temporal coding range can be large, the delay between EPSC and AP is quite reliable given a specific EPSC amplitude and a specific input phase. The Ap delays from Fig. 1*B* have a standard deviation (SD) with respect to the mean delay (black line) of only 7 ms, which corresponds to $\approx$13% of the temporal coding range. The root mean square SDs for the group data in Fig. 1*C* are 7 ms for $\psi = 170°$, 6 ms for $\psi = 140°$, and 7 ms for $\psi = 110°$. From these relatively small temporal jitters, we conclude that AP timing provides substantial information about the EPSC amplitude *A*. However, the transfer function $\Phi\psi(A)$ and thus probably also the amount of transmitted information critically depend on ψ. Next, we therefore investigate whether a large coding range (early ψ) or linearity of the transfer function (late ψ) is more beneficial for information transmission.

Transmission of Information from Synaptic Amplitudes to Spike Timing. To quantitatively assess the impact of the input phase ψ on the transmission of information, we measured AP phases Φ for 36 different input phases ψ. Fig. 2*A* depicts the obtained transfer functions $\Phi\psi(A)$, using a color code for the phase offset between postsynaptic AP and EPSC. The transfer functions show a window of opportunity (between $\approx$100° and 300°) that ensures both a sufficiently large coding range and an almost linear dependence on amplitude.

To obtain an efficient noise-free estimate of the transfer function $\Phi\psi(A)$, we applied EPSCs and oscillations to the conductance-based two-compartment model of a CA3 pyramidal cell by Pinsky and Rinzel (19) (Fig. 2*B* and *Materials and Methods*). The model accounts well for the experimental phenomenology from Fig. 1, and it allowed us to determine $\Phi\psi(A)$ as a function of ψ and *A* much more fine-grained (Fig. 2*C*) than in experiments (Fig. 2*A*). A comparsion between model and measured phase offsets indicates good qualitative agreement, especially for input phases $\psi \gtrsim 120°$.

The mutual information *I* between EPSC amplitude *A* and spike

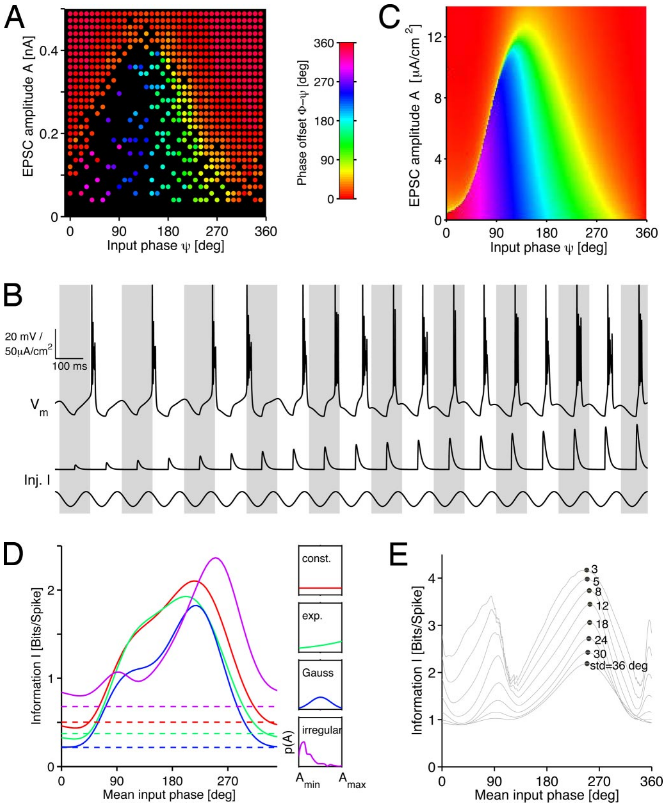

Fig. 2. Information transmission due to variations in EPSC amplitude and subthreshold oscillations. (*A*) Phase offsets $\Phi - \psi$ (color coded) between AP phase Φ and input phase ψ obtained from an exemplary experiment (10° resolution of input phases). (*B*) An input current (Inj. I) that combines oscillations and facilitating EPSCs leads to a precession of AP phases in a conductance-based two-compartment model. Here, EPSCs arrived at a phase angle of 180° after the peak of the subthreshold membrane potential oscillations. (*C*) Phase offset obtained from model simulations with a 0.1 $\frac{\mu A}{cm^2}$ resolution of EPSC amplitudes and a 2° resolution of input phases resembles the experimental data in *A*. (*D*) Mutual information *I* between AP phase Φ of the model and EPSC amplitude *A* reveals optimal mean input phases between ≈180° and 270°, depending on the amplitude statistics *p*(*A*). Four distributions *p*(*A*) are investigated: uniform (red), exponential (green), Gaussian (blue), and irregular (purple). Dashed lines mark amount of transmitted information without additional subthreshold oscillations. The SD of input times was taken as 30°/360° × 111 ms, which corresponds to a SD of 30° of the distribution p(ψ) of input phases for an oscillation frequency of 9 Hz. (*E*) Maximal information transmission (black dots) obtained with irregular amplitude distribution and subthreshold oscillations decreases by ≈50% for a 12-fold increase of the SD (labels) of *p*(ψ).

phase Φ (see *Materials and Methods*) was calculated by using the fine-grained transfer functions $\Phi\psi(A)$ from model simulations. The information I also depends on the distribution *p*(*A*) of EPSC amplitudes. We therefore calculated *I* for four input distributions of qualitatively different shapes (Fig. 2*D*): uniform, exponential, Gaussian, and evoked by irregular stimulation of the mossy fiber tract. As can be seen in Fig. 2*D*, *I* as a function of mean input phase $\bar{\psi}$ is similar for all four distributions *p*(*A*). Maximum information transmission, in general, requires late mean input phases $\bar{\psi} \gtrsim 200°$ that give rise to almost linear transfer functions $\Phi\psi(A)$. Therefore, strongly curved parts in $\Phi\psi(A)$, as obtained for early $\bar{\psi}$, are disadvantageous for information transmission given generic unimodal amplitude distributions. The highest information transmission we find for the distribution obtained from irregular stimulations of the mossy fiber tract that are motivated by *in vivo* spike train statistics of dentate gyrus granule cells (see *Materials and Methods* and refs. 20 and 21). The latter amplitude distribution exhibits a distinct peak at small amplitude values, at which the transfer function $\Phi\psi(A)$ has its highest sensitivity. In all cases, the subthreshold oscillations considerably enhance the maximum amount of transmitted information compared with simulations without oscillations (dashed lines in Fig. 2*D*).

To check how information transmission depends on the width of the distribution $p(\psi)$ of input phases, we calculated the information as a function of the SD of $p(\psi)$ (Fig. 2*E*). The maximal information increases from 2.2 bits per spike at SD = 36° to 4.2 bits at SD = 3° for the mossy fiber-evoked amplitude distribution. The optimal mean input phase $\bar{\psi}$ varies between 249° at SD = 3° and 254° at SD = 12°. Thus, the graph reveals the optimal mean input phase to be rather insensitive to the width of $p(\psi)$.

Temporal Compression and Discrimination Between Slow Temporal Patterns. The transmitted amount of information does not reveal how useful this information is to a downstream neuronal structure. As a proof of concept, we investigated the example of a downstream neuron (e.g., in CA1) that learns to discriminate between patterns of spike phases of a population of neurons (e.g., in CA3); see Fig. 3. These phase patterns are generated by much slower input patterns that may, for example, correspond to place-field activity evoked by a rat's path through a maze. In Fig. 3*A*, we show how synaptic facilitation can be used to compress a temporal pattern of spikes that are distributed over several seconds and across several input lines. We assume sparse patterns, i.e., each input line fires only once, to obtain as few subsecond correlations as possible. The slow temporal correlations between the different neurons in the population are stored in the memory traces provided by synaptic facilitation with a decay time constant of 5 s, as is known from the hippocampal mossy fiber synapse (13, 22). Synaptic facilitation, hence, acts as a short-term memory buffer. This buffer can be accessed by a readout stimulus, i.e., a synchronous activation of all input lines in combination with a subthreshold oscillation of the neurons' membrane potential. The resulting activity pattern is a temporally compressed reverse replay of the original pattern. The slow temporal pattern is thereby transferred to the time span of at most one oscillation cycle, which is 111 ms in our example (Fig. 3*A*). The peristimulus time histograms (PSTHs) of the temporal population patterns elicited by the readout stimulus at phase ψ are shown in Fig. 3 *B* and *E*. Depending on ψ, the PSTH can be unimodal for late and early input phases or bimodal for intermediate input phases ($50° < \psi < 200°$) (*cf.* Fig. 1 *C* and *D*).

To show how the compressed temporal pattern in a population of neurons can be discriminated by a downstream neuron (Fig. 3*C*), we trained a threshold unit, using the tempotron learning rule by Gütig and Sompolinsky (23) in the original parameter regime. The tempotron rule is a supervised learning rule extending the perceptron rule (*cf.* ref. 24) to the temporal domain (see *Materials and Methods*). Whereas the perceptron rule allows to learn a linear classification task on a set of temporally static patterns, the tempotron rule is able to learn a classification task in a spatiotemporal pattern space as shown in Fig. 3*A*. Because the decay time constant τ of the downstream EPSP has been identified as a crucial parameter for tempotron learning (23), we have conducted computer simulations for three different values of τ. The success of learning is illustrated in Fig. 3*D*, which depicts the percentage of correctly classified patterns as a function of the input phase ψ. The results strongly depend on τ. For downstream EPSPs with $\tau = 10$ ms, the tempotron rule performs best at an input phase of $\psi \approx 200°$. For $\tau = 20$ ms, an input phase of $\psi = 130°$ yields the best, although moderate, performance. For an even larger decay time constant $\tau = 30$ ms, there is, again, a distinct peak of the percentage of correctly classified patterns at $\psi = 70°$. A closer look at the PSTHs at these input phases (Fig. 3*E*) reveals three different paradigms: (*i*) High performance is found for flat PSTHs with a width of several times τ ($\psi = 200°$, $\tau = 10$ ms). This case can be considered as the original tempotron paradigm (23), in which most of the temporal informa-

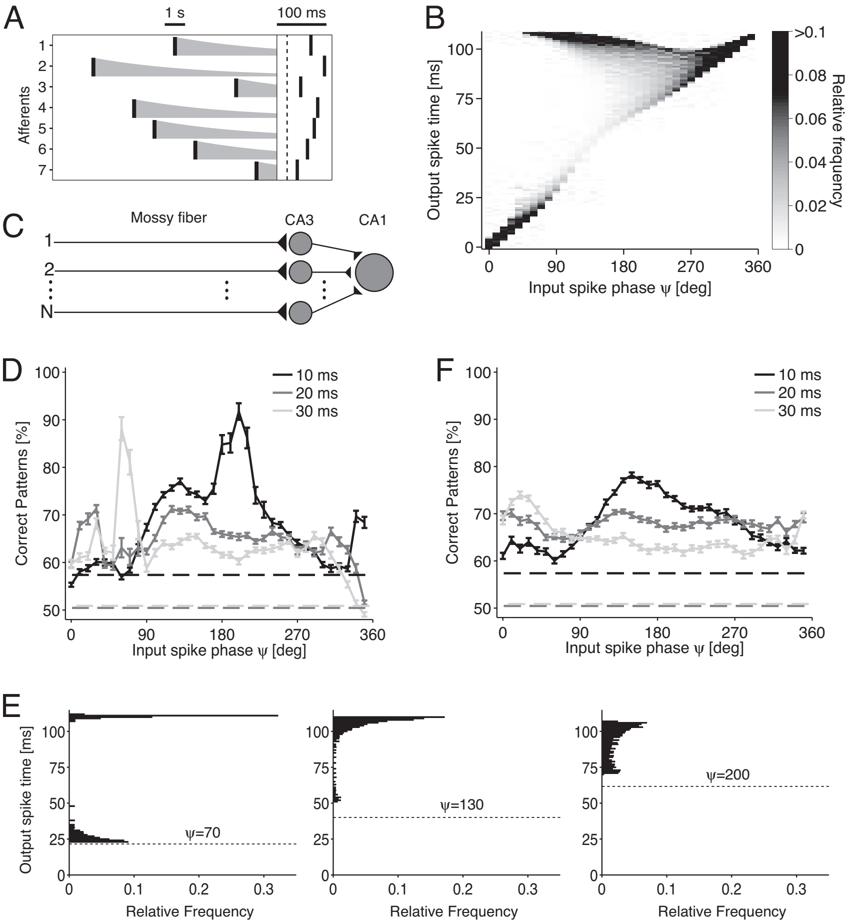

Fig. 3. Learning to discriminate between temporal patterns on a time scale of seconds. (*A*) Schematic illustration of temporal compression through synaptic facilitation. (*Left*) A temporal spike pattern (vertical bars) from a population of seven afferents on a time scale of seconds. The temporal pattern is preserved in the memory traces provided by the decay of synaptic facilitation (gray areas). (*Right*) Readout stimulus (dashed line) in combination with subthreshold oscillation evokes a reverse replay of the pattern in the seven neurons (vertical bars). Note different temporal scale bars for temporal pattern (*Left*) and reverse replay (*Right*). (*B*) Depending on the input phase ψ of the readout stimulus, the compressed population patterns show distinct phase distributions (gray-scale PSTHs). (*C*) A downstream threshold unit (e.g., in CA1) with adjustable synaptic weights learns to discriminate between temporally compressed phase patterns of a population of neurons (e.g., in CA3). (*D*) Fraction of correctly classified patterns after 100 learning cycles (mean ± SEM, $n = 50$ simulations) reveals an optimal input phase ψ that depends on the decay time constant τ of the downstream EPSP (gray levels depict different values of τ). Dashed lines indicate fractions of correctly classified patterns for simulations without subthreshold oscillations. Standard errors for dashed lines are all smaller than 0.7%. (*E*) Exemplary PSTHs from *B* for input phases $\psi = 70°$, 130°, and 200° (dashed lines), which yield best learning performance for the different time constants τ from *D*. (*F*) Adding a jitter (SD 30°) to the phase of the readout stimulus reduces performance of learning. Dashed lines are the same as in *D*, because there is no phase jitter without an oscillation.

tion is conveyed via the decaying slopes of the EPSPs. (*ii*) Learning can be moderately successful if the PSTH reveals a single peak that is narrower than the EPSP ($\psi = 130°$, $\tau = 20$ ms). In this regime, the learning rule thus also extracts temporal information from the rising slope of the EPSP. (*iii*) Finally, successful learning occurs for bimodally peaked PSTHs ($\psi = 70°$, $\tau = 30$ ms). In this case the temporal domain of the input pattern can be considered to be divided into two intervals (corresponding to high and low synaptic amplitudes) with peaked unimodal PSTHs each. As in the previous case, the temporal information with the two subgroups is again also conveyed via the rising slopes of the EPSPs.

In a final series of simulations, we jittered the phase of the readout stimulus (Fig. 3*F*). There, the general dependence on input phase is preserved compared with the noiseless case, although the peak performances are strongly reduced. Interestingly, the moderate performance peaks for a unimodal PSTH ($\psi = 130°$) are almost unchanged.

To summarize, the success of the tempotron rule strongly depends on properties of the downstream neuron such as the decay time constant τ of the EPSP. Moreover, using a model without subthreshold oscillations the success of learning is much smaller (dashed lines in Fig. 3 *D* and *F*). Thus, subthreshold oscillations that increase the temporal coding range can improve or, as in the present example, may even be inevitable to enable learning.

Discussion

The present article elucidates how short-term synaptic plasticity can contribute to the temporal compression of slow behaviorally induced temporal patterns. The core idea is to map the temporal input pattern to a pattern of EPSC amplitudes. The memory time constant of synaptic short-term plasticity thereby determines the time window over which the slow temporal patterns can extend. To obtain a broad (high entropy) distribution of EPSC amplitudes, the interval distribution of presynaptic inputs has to match the time constant of short-term plasticity. Subthreshold oscillations with a period much shorter than the memory time scale of short-term plasticity have been used to efficiently translate the synaptic amplitudes into a temporal sequence of action potentials in a population of neurons. This temporal sequence of APs provides temporal correlations on a shorter time scale, which are suitable to trigger long-term synaptic plasticity and learning.

In vitro experiments and a computational model reveal that the major contribution of subthreshold oscillations is to considerably increase the range for temporal encoding (Fig. 1 and *SI Appendix*, Fig. 1), and that the input phase ψ of the synaptic currents is a crucial parameter. For late input phases $\psi \approx 180°$, the AP (firing) phase is an only slightly curved function of the EPSC amplitude A, whereas for early input phases $\psi \lesssim 120°$ this transfer function is strongly curved (Fig. 1 *C* and *D*). However, late input phases provide a smaller possible range of temporal coding than early input phases, because the AP phases are confined to the interval between the input phase and the peak of the subthreshold oscillation at 360°. We find that EPSC amplitude information is best transformed into the phase of hippocampal CA3 pyramidal cell APs if the mean input phase is ≈250° (Fig. 2). The transmission of information is particularly high if we use EPSC amplitude statistics evoked by irregular *in vivo*-like activity patterns. In a further set of computer simulations, we have shown that a downstream neuron in CA1 can learn to discriminate between the temporally compressed spike patterns of a population of model CA3 pyramidal cells (Fig. 3). As an example for temporal compression, we have considered oscillations with a period of 111 ms and facilitation time constants of several seconds. These time scales match the typical period of hippocampal theta oscillations (4–12 Hz) (14) and the decay of facilitation at the mossy fiber synapse (13, 22), respectively. The long synaptic time scale provides a substrate for encoding behavioral events. Subthreshold theta oscillations allow a temporal compression to a much shorter time scale that is suitable to induce long-term synaptic changes. As with information transmission, subthreshold membrane potential oscillations also improve the performance of learning. However, whereas optimal information transmission requires EPSC inputs at phases that mostly avoid the strongly curved parts of the transfer function $\Phi\psi(A)$ (Fig. 2*D*), these parts can be helpful for learning. The input-phase dependence of learning is strongly modulated by EPSP decay time constant of the downstream neuron. In general, successful learning requires the downstream EPSP to be adjusted to the PSTH of the population pattern. The results on optimal input phases for learning are thus not generic, in the sense that they are derived for a specific learning paradigm with a given kinetics of the EPSPs, a given period length and shape of the subthreshold oscillation (10), and a given realization of the learning algorithm (23). Nevertheless, these results provide an example in which an optimal temporal code more strongly depends on downstream neuronal properties than on maximizing the transmission of information.

The temporally compressed firing pattern in the population of CA3 cells occurs in reversed order compared with the slow original one. This reversal is independent of whether the replay occurs with or without subthreshold oscillations. Interestingly, such reverse replay of place field activity in the hippocampus was predicted by Buzsáki (31) and recently also experimentally confirmed (32, 33). If this hippocampal reverse replay was a result of mossy fiber synaptic facilitation, our model predicts that instances of reverse replay should be temporally correlated with synchronous readout of the state of facilitation—the synaptic memory buffer—of a large number of mossy fiber synapses, as indicated by the dashed lines in Fig. 3*A*. This would correspond to the synchronous activation of a large fraction of the presynaptic dentate gyrus granule cells.

The firing pattern generated by facilitating inputs as shown in Fig. 1 is similar to hippocampal phase precession (25–29) if we associate the EPSC amplitude with the animal's place on a linear track. Synaptic facilitation of mossy fiber synapses at the interface between dentate gyrus and hippocampal CA3 pyramidal cells might thus provide an explanation for hippocampal phase precession (18). The underlying mechanism may principally apply to all synapses exhibiting short-term facilitation, as, e.g., in the entorhinal cortex (30). In addition to facilitation of excitatory synaptic transmission, short-term depression of inhibitory inputs results in a net increase of postsynaptic current amplitudes and, therefore, could account for the same phenomenon.

Besides theta–frequency oscillations, oscillations at higher frequencies, e.g., in the gamma range (34), with a period of tens of milliseconds could produce temporal codes if combined with short-term synaptic plasticity with memory time constants in the range of several hundreds of milliseconds. The latter time scale corresponds to short-term synaptic plasticity as reported for neocortical neurons (35, 36) and hippocampal CA1 pyramidal cells (37). Hence, the proposed mechanism is a temporal compression device mapping input correlations from any time scale of dynamical synaptic transmission to spike correlations on a time scale of the respective oscillation cycle.

Materials and Methods

Slice Preparation and Recordings. Hippocampal slices were obtained from 15- to 26-day-old Wistar rats. Preparation and recordings were done following standard procedures described in *SI Methods* in *SI Appendix*.

Simulated EPSCs and Oscillations. In the current–clamp experiments shown in this article, CA3 pyramidal cells were held at membrane potentials between −55 and −48 mV (junction potential ≈10 mV not corrected) by positive current injection. These values are in about the same range as the resting potentials of CA1 pyramidal cells *in vivo* (17). We applied artificial EPSCs $I_{syn}(t) = A\,[\exp(-t/\tau_1) - \exp(-t/\tau_2)]\,\Theta(t)$ that approximate the kinetics described for EPSCs in CA3 pyramidal cells evoked by putative single mossy fiber stimulation (11, 12), using a rise time of $\tau_2 = 1.5$ ms and a decay time of $\tau_1 = 10$ ms. The amplitude A of the artificial EPSC takes different values depending on the state of dynamical synaptic transmission. The current amplitudes A are varied between 0 and 600 pA, which corresponds to about the range of mossy fiber currents (12, 13). The function $\Theta(t)$ denotes the Heaviside step function, $\Theta(t) = 1$ for $t \geq 0$, and $\Theta(t) = 0$ otherwise.

In addition to EPSCs, subthreshold membrane potential oscillations were induced by the current input $I_{osc}(t) = I_1 \cos(2\pi f_\theta t)$, in which the theta frequency was chosen as $f_\theta = 9$ Hz, a typical value observed in freely behaving rats (14). The amplitude I_1 was adjusted (from 40 to 120 pA) such that the amplitude of the subthreshold membrane potential oscillation was ≈5 mV, similar to values recorded in anesthetized and freely moving animals (15).

Definition of AP Phases. The phase Φ of the postsynaptic APs was measured relative to the peaks of the membrane potential oscillations. These peaks were determined from an average of five oscillation cycles without additional EPSCs. Thus, phase zero corresponds to the maximum of the intracellular membrane potential oscillation, which, in the hippocampus, coincides with the trough of the *in vivo* extracellular local field potential in stratum pyramidale (14).

From $n = 21$ applications of stimulation protocols with combined oscillatory and EPSC currents, we determined a phase shift of 62 ± 8° (mean ± SD) between current oscillation I_{osc} and membrane potential oscillations. Each protocol contained at least 10 repetitions of the stimulus. Whenever we had to pool phase data over several cells (Fig. 1 *C* and *F*), we corrected input and firing phases with a constant phase shift of 60°.

Irregular Mossy Fiber Stimulation. The distribution of mossy fiber response amplitudes as used in Fig. 2*D* was determined as follows: The mossy fiber tract in hippocampal slices of postnatal day (P)21–P35 mice was extracellularly stimulated by using a saline-filled, low-resistance patch pipette positioned in the granule cell layer or hilar region. Stimulation was irregular and resembled the statistics of natural spike trains from dentate gyrus granule cells (20, 21). Stimulus trains followed an interstimulus interval (ISI) distribution where the probability of an ISI was proportional to 1/ISI with minimal, median, and maximal ISIs of 50 ms, 1.5 s, and 50 s, respectively. The resulting postsynaptic responses were recorded in whole-cell voltage-clamp configuration of CA3 pyramidal cells at a holding potential of −60 mV performed at room temperature. Comparable dynamics were measured by using field potential recordings both at room temperature and at 34°C (see ref. 13). The distribution shown in Fig. 2*D* is derived from $n = 6$ cells.

Mutual Information. The sensitivity of the AP phase Φ on changes of the EPSC amplitude A is quantified by the mutual information

NEUROSCIENCE

$$I = \int_{A_{\min}}^{A_{\max}} \mathrm{d}A p(A) \int_0^{360^\circ} \mathrm{d}\Phi p(\Phi|A) \mathrm{lg}_2 \left[\frac{p(\Phi|A)}{\int_{A_{\min}}^{A_{\max}} \mathrm{d}A' p(\phi|A') p(A')} \right]$$

between Φ and A. We therefore require a model of the amplitude distribution p(A) and the conditional probability $p(\Phi|A)$ of having Φ, given A. The latter distribution is obtained through $p(\Phi|A) = \int_0^{360^\circ} \mathrm{d}\psi p(\psi)\delta(\Phi - \Phi\psi(A))$, in which the phase transfer function $\Phi\psi(A)$ is derived from the two-compartment model (19) (see Fig. 2). The distribution $p(\psi)$ of input phases is assumed to be Gaussian with mean phase $\bar{\psi}$. Unless stated otherwise, the standard deviation of $p(\psi)$ was set to the exemplary value of 30°. The minimal and maximal EPSC amplitudes were $A_{\min} = 0 \frac{\mu A}{cm^2}$ and $A_{\max} = 14 \frac{\mu A}{cm^2}$, respectively.

Model. Computer simulations made use of a two compartment neuron model of a CA3 pyramidal cell by Pinsky and Rinzel (19). The model consists of a somatic and a dendritic compartment. The somatic compartment contains the standard Hodgkin–Huxley-type inactivating sodium and potassium delayed-rectifier currents. The dendritic compartment contains a calcium current, a potassium-mediated slowly activating afterhyperpolarization (AHP) current, and a fast activating potassium-mediated current, the saturation of which is calcium-dependent. The model has been extensively studied (e.g. ref. 38) and can be considered as one of the standard models for CA3 pyramidal cells.

The external currents applied to the model have the same shape as I_{osc} and I_{syn} in the electrophysiological recordings (see *Simulated EPSCs and Oscillations*). The amplitude of the oscillatory current was $I_1 = 2 \frac{\mu A}{cm^2}$, resulting in an amplitude of ≈5 mV for the membrane potential oscillation. The firing threshold was adjusted by an additional application of a constant current of $I_0 = -0.3 \frac{\mu A}{cm^2}$ to prevent firing for EPSP amplitudes $A = 0$. For simulations without subthreshold oscillations (dashed lines in Fig. 2*D*), we chose $I_1 = 0$ and $I_0 = -2.3 \frac{\mu A}{cm^2}$, which lead to a maximal delay of 70 ms between EPSC onset and AP. The model was implemented in C programming language. Integration was performed by using a fourth-order Runge–Kutta algorithm with adaptive step size (39).

Temporal Pattern Learning. We have defined 200 firing patterns of a population of 200 input lines such that each pattern contains one event (spike or burst) per input line occurring independently at random times t_n^{in} (n = 1, . . ., 200) in the interval between 0 and 10 seconds. Each input event triggers the maximal facilitation $A_{\max} = 14 \frac{\mu A}{cm^2}$ of the synapse connected to the specific input line. The facilitation f_n then decays exponentially with a time constant $\tau_f = 5$ seconds (Fig. 3*A*). To read out the states of facilitation, all synapses are simultaneously activated at a phase angle ψ with respect to an additional subthreshold oscillation with period 111 ms. The larger the delay between an input event and the readout stimulus, the smaller is the value of the facilitation f_n of the synapse at the time of readout. The readout stimulus therefore triggers a reverse replay of the pattern, and the replayed pattern is temporally compressed. The AP phases are obtained from the transfer function $\Phi\psi(A = f_n)$ depicted in Fig. 2*C*. The reversed and compressed pattern is then conveyed to a threshold unit and there elicits standardized EPSPs w_n ($e^{-t/\tau} - e^{-t/\tau_s}$) (for $t \geq 0$) with a membrane time constant τ, a synaptic time constant $\tau_s = \tau/4$, and a synaptic weight w_n.

Half of the above patterns were randomly classified as ''+'' patterns, the others are termed ''−'' patterns. The synaptic weights are trained via the tempotron learning rule (23) such that the threshold unit emits a spike for + patterns and does not fire for − patterns. Unless stated otherwise, all parameters were taken as proposed by Gütig and Sompolinsky (23). In particular, in each learning cycle, all patterns were presented in the same order. Learning was stopped when 100% of the patterns were classified correctly or when the maximal number of learning cycles (here 100) was exceeded. Simulations were run for different EPSP time constants τ and different input phases ψ of the readout stimulus. We repeated simulations 50 times for each set of parameters. For the simulation results shown in Fig. 3*D*, the phase ψ of the readout stimulus was drawn from a normal distribution with mean $\bar{\psi}$ and standard deviation of 30°.

ACKNOWLEDGMENTS. We thank Patrick Nicholson for providing insights into the analysis of intracellular oscillations and Jonas Rose for comments on the manuscript. This work was supported by the Deutsche Forschungsgemeinschaft Grants SFB 618 ''Theoretical Biology'' and GRK 1123 ''Memory Consolidation'' and Emmy Noether Grants Schm 1381/3,4 and Ke 788/1–2,3 (to D.S. and R.K.) and the Bundesministerium für Bildung und Forschung (Bernstein Centers for Computational Neuroscience Berlin and Munich) Grants 01GQ0410 and 01GQ0440.

1. Netoff TI, *et al.* (2005) Synchronization in hybrid neuronal networks of the hippocampal formation. *J Neurophysiol* 93:1197–1208.
2. Bendels MHK, Leibold C (2007) Generation of theta oscillations by weakly coupled neural oscillators in the presence of noise. *J Comput Neurosci* 22:173–189.
3. Traub RD, Whittington MA, Colling SB, Buzsáki G, Jefferys JG (1996) Analysis of gamma rhythms in the rat hippocampus *in vitro* and *in vivo*. *J Physiol* 493:471–484.
4. Memmesheimer RM, Timme M (2006) Designing the dynamics of spiking neural networks. *Phys Rev Lett* 97:188101.
5. Markram H, Lubke J, Frotscher M, Sakmann B (1997) Regulation of synaptic efficacy by coincidence of postsynaptic APs and EPSPs. *Science* 275:213–215.
6. Bi GQ, Poo M-M (1998) Synaptic modifications in cultured hippocampal neurons: Dependence on spike timing, synaptic strength, and postsynaptic cell type. *J Neurosci* 18:10464–10472.
7. Kempter R, Gerstner W, van Hemmen JL (1999) Hebbian learning and spiking neurons. *Phys Rev E* 59:4498–4514.
8. Zucker RS, Regehr WG (2002) Short-term synaptic plasticity. *Annu Rev Neurosci* 64:355–405.
9. Nicoll R, Schmitz D (2005) Synaptic plasticity at hippocampal mossy fibre synapses. *Nat Rev Neurosci* 6:863–876.
10. Hopfield JJ (1995) Pattern recognition computation using action potential timing for stimulus representation. *Nature* 376:33–36.
11. Jonas P, Major G, Sakmann B (1993) Quantal components of unitary EPSCs at the mossy synapse on CA3 pyramidal cells of rat hippocampus. *J Physiol* 472:615–663.
12. Toth K, Suares G, Lawrence JJ, Philips-Tansey E, McBain CJ (2000) Differential mechanisms of transmission at three types of mossy fiber synapse. *J Neurosci* 20:8279–8289.
13. Gundlfinger A, *et al.* (2007) Differential modulation of short-term synaptic dynamics by long-term potentiation at mouse hippocampal mossy fibre synapses. *J Physiol* 585.3:853–865.
14. Buzsáki G (2002) Theta oscillations in the hippocampus. *Neuron* 33:325–340.
15. Kamondi A, Acsady L, Wang XJ, Buzsáki G (1998) Theta oscillations in somata and dendrites of hippocampal pyramidal cells *in vivo*: activity-dependent phase-precession of action potentials. *Hippocampus* 8:244–261.
16. Bland BH, Konopacki J Dyck R (2005) Heterogeneity among hippocampal pyramidal neurons revealed by their relation to theta-band oscillation and synchrony. *Exp Neurol* 195:458–474.
17. Lee AK, Manns ID, Sakmann B, Brecht M (2006) Whole-cell recordings in freely moving rats. *Neuron* 51:399–407.
18. Thurley K, Leibold C, Gundlfinger A, Schmitz D, Kempter R (2008) Phase precession through synaptic facilitation. *Neural Comput*, 10.1162/neco.2008.07.06-292.
19. Pinsky PF, Rinzel J (1994) Intrinsic and network rhythmogenesis in a reduced Traub model for CA3 neurons. *J Comput Neurosci* 1:39–60.
20. Mizumori SJ, McNaughton BL, Barnes CA (1989) A comparison of supramammillary and medial septal influences on hippocampal field potentials and single-unit activity. *J Neurophysiol* 61:15–31.
21. Jung MW, McNaughton BL (1993) Spatial selectivity of unit activity in the hippocampal granular layer. *Hippocampus* 3:165–182.
22. Salin PA, Scanziani M, Malenka RC, Nicoll RA (1996) Distinct short-term plasticity at two excitatory synapses in the hippocampus. *Proc Natl Acad Sci USA* 93:13304–13309.
23. Gütig R, Sompolinsky H (2006) The tempotron: A neuron that learns spike timing-based decisions. *Nat Neurosci* 9:420–428.
24. Hertz J, Krogh A, Palmer RG (1991) *Introduction to the Theory of Neural Computation.* (Westview, Boulder, CO).
25. O'Keefe J, Recce ML (1993) Phase relationship between hippocampal place units and EEG theta rhythm. *Hippocampus* 3:317–330.
26. Skaggs WE, McNaughton BL, Wilson MA, Barnes CA (1996) Theta phase precession in hippocampal neuronal populations and the compression of temporal sequences. *Hippocampus* 6:149–172.
27. Mehta MR, Lee AK, Wilson MA (2002) Role of experience and oscillations in transforming a rate code into a temporal code. *Nature* 417:741–746.
28. Harris KD, *et al.* (2002) Spike train dynamics predicts theta-related phase precession in hippocampal pyramidal cells. *Nature* 417:738–741.
29. Huxter J, Burgess N, O'Keefe J (2003) Independent rate and temporal coding in hippocampal pyramidal cells. *Nature* 425:828–832.
30. Gloveli T, Schmitz D, Empson R, Heinemann U (1997) Frequency-dependent information flow from the entorhinal cortex to the hippocampus. *J Neurophysiol* 78:3444–3449.
31. Buzsáki G (1989) Two-stage model of memory trace formation: A role for ''noisy'' brain states. *Neuroscience* 31:551–570.
32. Diba K, Buzsáki G (2007) Forward and reverse hippocampal place-cell sequences during ripples. *Nat Neurosci* 10:1241–1242.
33. Foster DJ, Wilson MA (2006) Reverse replay of behavioural sequences in hippocampal place cells during the awake state. *Nature* 440:680–683.
34. Buzsáki G, Draguhn A (2004) Neuronal oscillations in cortical networks. *Science* 304:1926–1929.
35. Tsodyks MV, Markram HD (1997) The neural code between neocortical pyramidal neurons depends on neurotransmitter release probability. *Proc Natl Acad Sci USA* 94:719–723.
36. Varela JA, *et al.* (1997) A quantitative description of short-term plasticity at excitatory synapses in layer 2/3 of rat primary visual cortex. *J Neurosci* 17:7926–7940.
37. Dobrunz LE, Stevens CF (1999) Response of hippocampal synapses to natural stimulation patterns. *Neuron* 22:157–166.
38. Booth V, Bose A (2001) Neural mechanisms for generating rate and temporal codes in model CA3 pyramidal cells. *J Neurophysiol* 85:2432–2445.
39. Press WH, Teukolsky SA, Vetterling WT, Flannery BP (1992) *Numerical Recipes in C* (Cambridge Univ Press, Cambridge, UK).